



King's Research Portal

DOI:

10.1016/j.ymeth.2016.11.005

Document Version Publisher's PDF, also known as Version of record

Link to publication record in King's Research Portal

Citation for published version (APA):

Staszowska, A. D., Fox-Roberts, P., Foxall, E., Jones, G. E., & Cox, S. (2017). Investigation of podosome ring protein arrangement using localization microscopy images. *Methods*, *115*, 9-16. https://doi.org/10.1016/j.ymeth.2016.11.005

Please note that where the full-text provided on King's Research Portal is the Author Accepted Manuscript or Post-Print version this may differ from the final Published version. If citing, it is advised that you check and use the publisher's definitive version for pagination, volume/issue, and date of publication details. And where the final published version is provided on the Research Portal, if citing you are again advised to check the publisher's website for any subsequent corrections.

General rights

Copyright and moral rights for the publications made accessible in the Research Portal are retained by the authors and/or other copyright owners and it is a condition of accessing publications that users recognize and abide by the legal requirements associated with these rights.

- •Users may download and print one copy of any publication from the Research Portal for the purpose of private study or research.
- •You may not further distribute the material or use it for any profit-making activity or commercial gain •You may freely distribute the URL identifying the publication in the Research Portal

If you believe that this document breaches copyright please contact librarypure@kcl.ac.uk providing details, and we will remove access to the work immediately and investigate your claim.

Download date: 01. Jan. 2025



Contents lists available at ScienceDirect

Methods

journal homepage: www.elsevier.com/locate/ymeth



Investigation of podosome ring protein arrangement using localization microscopy images



Adela D. Staszowska, Patrick Fox-Roberts, Elizabeth Foxall, Gareth E. Jones, Susan Cox*

Randall Division of Cell and Molecular Biophysics, King's College London, London, UK

ARTICLE INFO

Article history:
Received 15 August 2016
Received in revised form 4 November 2016
Accepted 7 November 2016
Available online 10 November 2016

Keywords: Podosomes Super-resolution microscopy Localization microscopy Image analysis Pattern recognition

ABSTRACT

Podosomes are adhesive structures formed on the plasma membrane abutting the extracellular matrix of macrophages, osteoclasts, and dendritic cells. They consist of an f-actin core and a ring structure composed of integrins and integrin-associated proteins. The podosome ring plays a major role in adhesion to the underlying extracellular matrix, but its detailed structure is poorly understood. Recently, it has become possible to study the nano-scale structure of podosome rings using localization microscopy. Unlike traditional microscopy images, localization microscopy images are reconstructed using discrete points, meaning that standard image analysis methods cannot be applied. Here, we present a pipeline for podosome identification, protein position calculation, and creating a podosome ring model for use with localization microscopy data.

© 2016 The Authors. Published by Elsevier Inc. This is an open access article under the CC BY license (http://creativecommons.org/licenses/by/4.0/).

1. Introduction

Super-resolution microscopy is the term given to a class of techniques which can image structures smaller than the diffraction limit (\sim 250 nm for visible light). Currently, localization microscopy is a highly popular method for achieving super-resolution due to its experimental simplicity. Localization microscopy is based on detection and localization of randomly activated single molecules in a sequence of images. These single molecule localizations are then used to reconstruct a super-resolution image [1,2]. This means that the reconstructed image is a collection of discrete points and should be considered as a data set rather than as an image.

Quantitative analysis of localization microscopy datasets requires identification of structures of interest in the data. Although pattern recognition is possible without a model of a structure, it is expensive computationally. Therefore it is easier to identify structures of interest either manually or by software using a set of rules, characteristics or a model of the structure. For example, a number of studies have discussed identification of the nuclear pore complex imaged with localization microscopy. This was done by creating an intensity profile from single molecule localizations and reconstructing. An average model was created either using localizations from many nuclear pore structures [3] or by convolving molecule localizations with a Gaussian to create a continuous image [4] and then identifying them.

E-mail address: susan.cox@kcl.ac.uk (S. Cox).

Here, we propose a method using the Ransac algorithm [5] and an application of the Hough transform [6] to analyze localization microscopy data to identify podosomes, which are matrix adhesive structures formed on the cell surface of a number of cell types (for example macrophages, osteoclasts, dendritic cells, and Srctransformed fibroblasts [7]). Podosomes consist of an f-actin core and a ring structure formed of integrin and integrin-associated proteins (for example vinculin, paxillin, and talin) [7]. Podosomes are thought to be involved in adhesion, tissue transmigration and cancer metastasis [8]. Adhesion to the extracellular matrix, one of the functions of podosomes, is moderated and maintained mainly by the podosome ring [7].

Podosome rings in standard resolution fluorescence microscopy images are visible as circles surrounding the actin-rich podosome cores, and their radius varies between 0.5 and 1 µm [9], with some evidence that diverse proteins are occupying discrete zones in the ring [10]. Recent studies using different super-resolution methods have presented two conflicting models of the podosome structure. The podosome ring was reported to have the shape of continuous hexagons in studies with high density localization microscopy methods using live and fixed samples expressing fluorescent proteins [11]. In contrast, when primary/secondary antibody labeled fixed samples were imaged with localization microscopy the ring was reported to be a collection of sparse protein clusters [10,12]. Results acquired using both of these approaches had suggested a specific protein arrangement in the ring. For example, a visual assessment of the images in [11] hinted that talin was closer to the podosome center than vinculin. This was partially confirmed by a

^{*} Corresponding author.

confocal microscopy study presented in [10], which found talin formed an inner ring close to the core, with vinculin being uniformly distributed through the podosome ring. However, a comparison of the relative positions of different protein-classes found between the two experimental approaches has not been possible due to a lack of analysis methods suitable for localization microscopy data.

Our analysis method, described below, is tailored to be used with localization microscopy datasets. It identifies podosomes using a model of podosome ring structure, calculates the podosome ring protein positions and uses those positions to create a second, more refined model of the podosome ring. Podosomes were identified using an approximate, circular model of the ring structure and for each identification the center point and radius was measured. For identified podosomes we calculated the average position of the protein around the ring. As the ring size varies between different podosomes, we looked at the relative distance of one protein to another to amass reliable statistics. Relative protein distances can then be used to build a podosome ring model.

2. Methods

2.1. Sample preparation

The podosome samples were prepared using the protocol presented in [13]. Conjugated tandem dyes were supplied by Oleg Glebov and prepared using the protocol presented in [14].

2.2. Imaging

Localization microscopy imaging was performed using the Nikon STORM system, with an Eclipse Ti-E Inverted Nikon Microscope, Andor Ixon camera, laser and LED light sources (laser wavelengths are: 405 nm, 30 mW; 488 nm, 90 mW; 561 nm, 90 mW and 647 nm, 170 mW) and operated with NIS Elements software with the N-STORM module. The imaging was performed with TIRF, 100x, N.A. 1.49 objective. In two color STORM imaging the 647 nm laser was set to 25 mW, the 488 nm to 18 mW, and the 561 nm to 18 mW. The laser power was adjusted during the acquisition to acquire similar number of counts in every frame (as far as possible), up to around 80% of the maximal laser power (72 mW for 488 nm, 561 nm, and 136 mW for 647 nm laser). As podosome rings are rather flat structures positioned at the cell membrane, imaging was performed in TIRF (or near-TIRF) angle to reduce background and improve the signal-to-noise ratio.

Prior to imaging samples were immersed in an imaging buffer. The base buffer was made according to the Nikon Protocols for sample preparation [14] with β -Mercaptoethylamine (MEA, Sigma Aldrich, 30070-50G). To ensure better stability of dyes in the samples Cyclooctatetraene (COT, 98%, Sigma Aldrich, 138924-1G) was dissolved in DMSO (Sigma Aldrich, 472301-1L-D) and added to the base buffer to a final concentration of 2 mM [15].

In each series about 10,000 frames were acquired, at a rate of 30–50 frames per second. An epi-fluorescent image of the region of interest was also captured (with LED light, 488 nm and 561 nm) for each localization microscopy acquisition, which was later compared with the reconstructed image. The superresolution images were reconstructed from the image sequences using QuickPALM [16]. The sample preparation, imaging and analysis for 3B microscopy was performed according to [11].

2.3. Podosome identification and protein position calculation

To identify podosomes, it was first necessary to create a model for them. We made a number of simplifications to the model which we used to identify the podosome ring structure. The ring was approximated to be circular (a circle's center and radius can be found using coordinates of three points positioned on that circle). After the podosome identification the relative positions of proteins in the podosome ring were calculated. Because some of the podosomes were elongated, and the podosome size varies, the distance between the podosome center and proteins positioned in the ring is not constant between podosomes or even a single protein in one podosome ring. Thus the protein positions were calculated relative to each other by subtracting the average position of one protein from the average position of another.

The podosome rings were identified using a circular model. The equation of a circle passing through three points can be found using Eq. 1. Here we were interested in identifying the circle center and the radius of the fitted circle (see Section 3). The software randomly selected three points (separated by a small enough distance so they could confidently belong to a single podosome ring) from the localization data set (see step 1 in Fig. A.1) [5]. Then the circle center and radius were calculated (step 2 in Fig. A.1). The fitted circle was then examined to meet two criteria: the size of the fitted circle had to be similar to the size of actual podosomes (radius $0.5-1 \mu m$) and the inside of the circle should have a very small number of localizations, because there should be no fluorophores present in the podosome cores. The acceptable number of localizations in the podosome center was established by finding the density of background localizations and then setting the threshold 50% higher (usually the same value was used for analysis datasets of the same type). Lastly, the overlap of the fitted circle with the actual podosome ring structure was evaluated, by examining the distribution of protein localizations surrounding the fitted circle in a proximity corresponding to an actual podosome ring thickness (\sim 400 nm). The values used for this fitting step were established experimentally based on a fit to an average podosome ring from a localization microscopy dataset (step 3 in Fig. A.1). If these criteria were met the fitted circle parameters were saved (step 4 in Fig. A.1), if not they were discarded. Then a new set of three points was chosen and circle fitting steps were repeated (steps 1-3 in Fig. A.1). The circular model is optimal for the rounder podosomes. For elongated (elliptical) podosomes the fitted circle centers provided a wider range of possible podosome center points resulting in an elongated distribution (this can be seen for some podosomes in Fig. B.2b and c). Usually circles are fitted across the whole image, however, their density is much higher in areas with podosomes

The software ran for a set number of repetitions, which was arbitrarily selected to be around 100x higher than number of points in the data. The repetition number was smaller than the number of possible combinations of selecting three points, however it usually provided about 3000 circle fittings meeting the filtering criteria. For a data set containing up to twenty podosomes this provided a good range of possible podosome centers. The centers of fitted circles were saved and plotted in an image for reference (see Fig. B.2). The podosome centers were found using an application of the Hough transform [6]. The center points of the fitted circles were convolved with a Gaussian function. Then, the central points of actual podosomes were found by finding the local maxima (step 5 and 6 in Fig. A.1 and B.2). Compared with the visual assessment of the data the software had 80% success rate (the remaining 20% were false positives and negatives, which were removed during the protein distance calculation, see Fig. B.2).

The protein positions in the podosome ring were calculated relative to each other, comparing the average position of one protein to the second. The podosome centers were used for the protein distance calculation. The outer boundary of the podosome ring was usually hard to define computationally because of background noise and close proximity between podosomes, although the rings boundaries are clearly visible to the human eye (see Fig. B.1). Thus a user input was required at this stage to create a mask image

marking podosome boundaries. These images were created in black-and-white, where white marked areas with podosomes (step 1 in Fig. A.2). Use of masking images had an additional advantage of excluding areas where podosome ring composition may be different. For example fragments of the ring shared by two joint podosomes and removing false positive podosome identifications (see Appendix B).

The podosome ring shape can sometimes be elongated, and so the proteins in the ring may not be equally spaced from the podosome center. Thus, the calculations of relative positions were performed for small sections of the ring the angular increment for each section was set to 5.7°. The increment value was selected to get on average about ten localizations of each protein in the segment (step 2 in Fig. A.2). The calculated average difference in positions of the two proteins in each segment was then weighted by the number of points in given segment – so the regions with small numbers of localizations would not influence strongly the end result (step 3 in Fig. A.2).

3. Equation of the circle passing through three points

There is exactly one circle passing through three points (x_1, y_1) , (x_2, y_2) , (x_3, y_3) which are not positioned on the same line. This

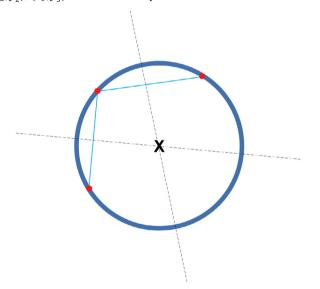
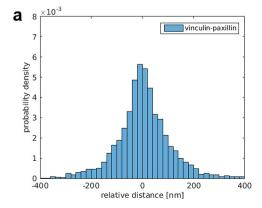


Fig. 1. A geometrical construction of a circle passing through three points. If we draw two perpendicular lines crossing the segments connecting points, then their crossing point will be the center of the circle.



circle can be constructed geometrically by drawing two perpendicular lines crossing the segments between points, their crossing point will be the center of the circle or arithmetically using equation of a circle:

$$(x - x_0)^2 + (y - y_0)^2 = r^2 \tag{1}$$

By solving Eq. 1 using three points positioned on the circle we found coordinates of the central point. The circle radius was later found by calculating distance between the circle center point and any of the three points on the circle (Fig. 1).

4. Results

The methodology developed for podosome ring analysis was used to acquire preliminary results of protein positions in the podosome ring. The relative positions of vinculin-paxillin and vinculintalin were calculated. Vinculin and paxillin data sets were collected using samples stained using tandem dye pairs and imaged using Nikon N-STORM system. The talin-vinculin pair was imaged using samples prepared with mCherry-talin construct and stained with Alexa Fluor 488 (see [11] for details). The relative positions of two proteins in each pair were calculated (see Section 2.3). The resulting distributions of relative distance measurement are shown in Fig. 2. For the vinculin-paxillin pair around 380 podosomes (from four samples, Fig. 1a) and for the talin-vinculin pair 159 podosomes from a single data set were analyzed (see Fig. 1b).

The results distribution for vinculin-paxillin is symmetric and it has a very sharp peak and weak tails. Mean, median, standard deviation and the 1st and 3rd quartiles were calculated for the results distribution (see Table 1). The central tendency of this distribution suggests a very small difference between positions of vinculin and paxillin. The mean value is equal to 4 nm and median 1 nm, suggesting that the paxillin is located further from the podosome core than vinculin. However, the mean and median values are still too small to provide a definitive answer about protein arrangement. The central tendency is smaller than the proteins size (minimal protein size was calculated using methodology presented in [17], see Table C.1).

Use of fluorescent proteins expressed directly by the protein of interest can remove the issue of the localization error due to distance between the detected fluorescent marker and marked protein, because they are expressed directly into the protein of interest. However, the quantum yield of the fluorescent proteins is smaller than that of organic dyes resulting in lower intensity and more dense data sets. Analysis of denser data sets requires more time and specially designed analysis methods for Example 3B [11]. Datasets with two of the podosome ring proteins vinculin

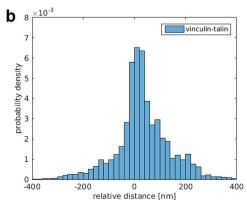


Fig. 2. Histograms of the position difference between two analyzed proteins from podosome rings. (a) The relative position was calculated as difference between the average position of paxillin from the vinculin position. For positive values paxillin is closer to the podosome core, for negative vinculin is closer. (Results for data sets acquired with standard localization microscopy.) (b) The relative positions of talin and vinculin (calculated by subtracting average talin position from vinculin position). For positive values talin is closer to the podosome center, where for negative vinculin is closer. (Results for 3B method analyzed images).

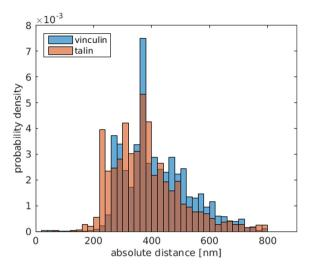


Fig. 3. Histograms of the absolute positions of talin and vinculin in podosome rings. Absolute positions were calculated from the podosome center.

stained with Alexa Fluor 488 and talin marked with mCherry was imaged and analyzed using 3B method [11]. Analysis of 159 podosomes was performed to measure relative distance of talin and vinculin (measured as a difference between average vinculin position and average talin position). The relative positions of talin in respect to vinculin (see Fig. 1b) and absolute protein positions (see Fig. 3) were calculated.

An analysis of more than 150 podosome rings provides an indication into talin and vinculin positions in the podosome ring. The relative position measurements indicated that on average talin is 33 nm closer to the podosome center than vinculin. When considering median value the relative distance is 24 nm. It is possible to analyze absolute distances of the protein positions in the ring, however, the podosome sizes in analyzed data should be similar.

Here, the absolute protein distances (measured from protein position to the podosome center) for talin and vinculin also suggest that talin is closer to the podosome core (see Fig. 3 and Table 2). We note that it is important to only compare measurements taken with the same technique as differences in the ring thickness could give rise to a bias in the measured radius (see Appendix D).

4.1. Discussion

We have presented a methodology for podosome identification and calculation of the relative position of different proteins in the ring. The podosome rings were identified in localization microscopy data using a circular model of podosome structure. Our method provides a success rate of 80% (similar to one delivered

Table 1Statistical parameters of distributions of relative protein distance calculations for vinculin-paxillin and vinculin-talin protein pairs.

| Protein pair | Mean relative distance [nm] | Median relative distance [nm] | Standard deviation | Quartiles |
|-------------------|--------------------------------|----------------------------------|-----------------------|-----------|
| Vinculin-paxillin | 4 | 1 | 110 | (-40, 30) |
| Vinculin-talin | 33 | 24 | 110 | (0, 100) |

 Table 2

 Statistical parameters of results distributions of absolute positions of talin and vinculin

| Protein | mean distance [nm] | Median distance [nm] | Standard deviation | Quartiles |
|----------|-----------------------|-------------------------|-----------------------|------------|
| Vinculin | 421 | 394 | 120 | (360, 500) |
| Talin | 388 | 366 | 131 | (300, 440) |

for podosome identification in confocal images [12]). Using podosome identifications the protein localized positions were used for calculations of relative protein distance. In order to build a complete model of the positions of different proteins the positions of vinculin, paxillin, and talin were compared with each other. This has enabled us to build up information about the average positions of these proteins in the podosome ring. Since we are looking at an average of the relative positions, this method allows us to use data from different localizations techniques. The data also yield absolute values, which show some difference between the standard localization and 3B methods for the same protein (see Fig. D.3). Resolving the origin of these differences will require the comparison of multiple labelling and super-resolution techniques in the future.

The varying qualities of the images resulting from different localization microscopy methods highlights that labelling, imaging and image analysis methods can have a strong impact on data quality and interpretation. The localization error can be caused by a number of factors, starting with the method used to tag proteins. The primary/secondary antibody construct separates the detectable organic dye from the protein [18]. The organic dyes are usually around 4 nm in size and the antibody length is around 5 nm, which means that the labeled protein localization can differ up to 9 nm from the organic dye [19]. For this study the proteins of interest were stained with tandem dye pairs which could potentially introduce even bigger distance between the protein of interest and the organic probe. Another issue is that, although the monoclonal primary antibody used for staining does attach to a specific location on the protein, the information about the exact attachment sequence is not readily available. With primary/secondary labeling systems there can be clustering artefacts, as more than one secondary can attach to each primary. Clustering artefacts can also be caused by the reappearance of single molecules. Although this affects the final number of molecules detected [19], it is less important for the average position measurements as reappearances are thought to be equally likely for all molecules. Additionally, the thickness of the ring and density of labelling can also influence a measurement of protein positions (see Appendix D). Lastly, each localized molecule position is estimated using information delivered by photons coming from the molecule. Thus, the molecule position is estimated with uncertainty caused by a limited number of photons detected and it is approximately inversely proportional to the square root of the number of photons detected [20], while the exact uncertainty of a localization can be found from the Fisher information limit [21].

Overall, our analysis method provided more precise measurements for data sets acquired for samples where at least one protein was marked with fluorescent protein and the second with organic dye. Previously discussed factors limiting accuracy for primary-antibody staining are limited by use of only one dye to mark the protein of interest (here vinculin). Use of more than one fluorescent protein to mark proteins in the podosome ring could lead to even more precise measurement. The main source of localization error – use of two antibodies to attach a fluorescent marker – would be removed, because fluorescent markers would be synthesized directly in the desired protein.

Most importantly the pipeline presented here is ready to be used for a complete analysis of podosome ring protein positions. More data sets will be required to map positions of vinculin, paxillin, and talin to reference their relative distance. It is also possible to use software presented here for identification and analysis of a wide range of other structures, imaged with localization microscopy, which have circular ring shape, for example the nuclear pore complex. Lastly, the pipeline can be used to identify structures with different shapes after implementation of a different model of structure. The new model would have to be optimized to best describe the analyzed structure.

Acknowledgements

The authors thank S. Mavadia, R. Szepietowski, and E. Rosten for early discussions, and O. Glebov for kindly supplying us with the tandem conjugated dyes. G.E.J and S.C were supported by the MRC (Next Generation Optical Microscopy Initiative Program Grant MR/K015664/1). S.C. by the BBSRC (Grant BB/K01563X/1) and S.C. is a Royal Society University Research Fellow. A.S. was funded by an EPSRC studentship and E.F. was funded by King's College studentship. The authors thank the Nikon Imaging Centre at King's College London, where localization microscopy data were acquired. The data supporting this research can be accessed using http://doi.org/10.18742/RDM01-101. For further information about the data please email the corresponding author or adela. staszowska@kcl.ac.uk.

Appendix A. Software flowcharts: Podosomes identification and protein distance calculation

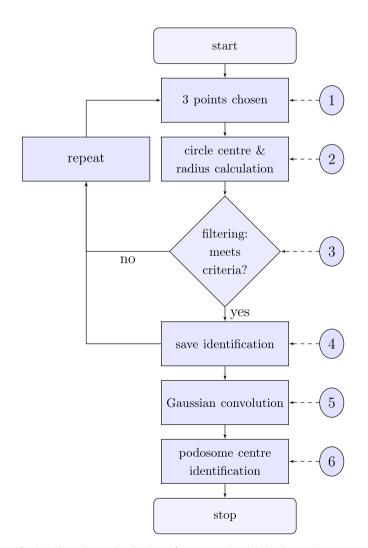


Fig. A.1. The podosome localization software operation. (1) The three points were selected randomly from the data set. (2) The radius and a center point of circle passing by three points were calculated. (3) Filtering step to check if the fitted circle was close to the properties of the podosome ring and sample. If the filtering criteria were met the circle center was saved (step 4) the steps 1–3 were repeated. Otherwise a new set of points was chosen (back to step 1). (5) The circle center positions were convolved with the Gaussian and saved as an image. (6) The podosome centers were found by identifying local maxima on the Gaussian image created in step 5.

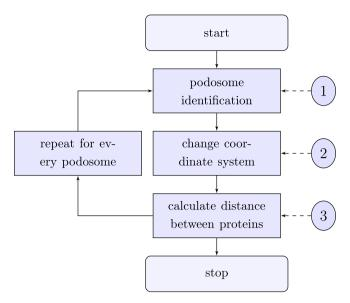


Fig. A.2. The operation of a program calculating positions of proteins in the podosome ring. The list of podosome centers made by the podosome center localization program is used. For every podosome center the points which belong to this podosome are identified using masking image (step 1). Then for an easier calculation the coordinate system was changed from Cartesian to polar coordinates (step 2) – the podosome center becomes a center of the polar coordinate system and, each point belonging to this podosome is described by the distance to the center and its angular position. The relative distance between two proteins was calculated and saved (step 3).

Appendix B. Podosome identification and localization microscopy images

Appendix C. The minimal protein volume and size

The minimal protein sizes were calculated according to the methodology presented in [17]. These calculations provide an estimation of the minimal size of the molecule and assume that it has a globular shape, however this is not true for a number of the proteins for example vinculin in its active state.

Appendix D. The measured ring radius

If the protein is evenly distributed through the podosome ring then the average position calculated will be slightly biased to the outer edge of the ring due to a higher number of molecules. However, if the fluorophores are equally likely to be anywhere on the ring then the outer side of the ring will have lower density of localizations than the inner side. Here, we have investigated how the size of this effect would vary with the ring thickness.

A number of datasets were simulated to account for the effect of sampling. Two sizes of inner rings with different thickness were simulated. These two types of rings correspond to the ratio of an average radius and thickness of the rings, observed using samples with two proteins labeled (here vinculin-paxillin) and one protein transfected and the second labeled (vinculin-talin). This ratio was estimated to be 0.6 (for vinculin-paxillin) and 0.1 (for vinculintalin). The points/single molecule localizations in the rings were simulated with an equal density (see Fig. D.1). The averaged measured and expected radius are presented in Figure D.2.

The simulation indicated that the localization density (sampling) can have an influence on the measured value of the ring radius. For thicker rings the difference between the measured and expected values are bigger than for a thinner radius. However, since in our measurements we make comparisons between

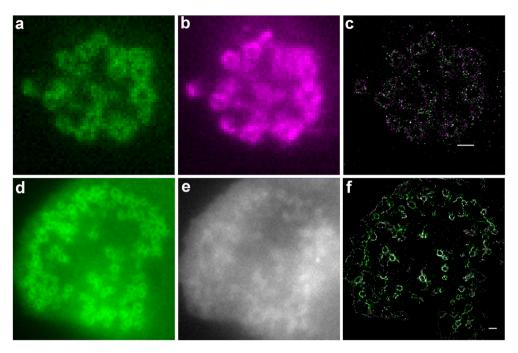


Fig. B.1. Super-resolution imaging of podosome samples. Top row: (a-b) Wide-field and super-resolution reconstructed images of the podosome rings labeled with tandem dyes. Vinculin (green) was labeled with Cy2-Alexa Fluor 647 and paxillin (magenta) with Cy3-Alexa Fluor 647. Bottom row: (d-e) Wide-field and (f) 3B reconstructed super-resolution image of the podosome rings. Vinculin (green) was labeled with Alexa Fluor 488 and talin (grey) was transfected with mCherry-talin construct. Scale bar: $1 \mu m$. (For interpretation of the references to colour in this figure legend, the reader is referred to the web version of this article.)

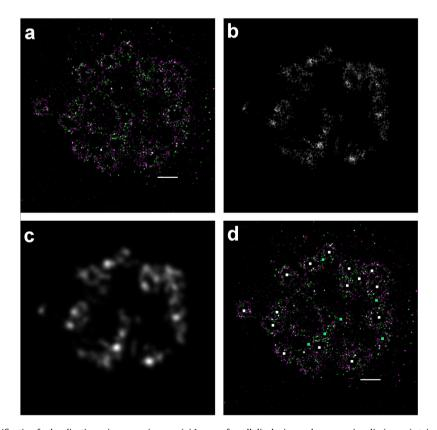


Fig. B.2. Podosome center identification for localization microscopy images. (a) Image of a cell displaying podosomes, vinculin (green) stained with Cy2-Alexa Fluor 647 and paxillin (red) with Cy3-Alexa Fluor 647. (b) Possible podosome centers found using the algorithm after applying filtration step (the image was blurred for improved visibility). (c) The center points were convolved with the Gaussian function. The actual centers of podosomes were found by identifying the local intensity maxima. (d) Identified podosome centers (marked with squares) displayed over the localization microscopy image of the podosome rings. White squares mark correct podosome identifications, green squares false positives, and white arrows false negatives (not identified podosomes). Scale bar 1 μ m. (For interpretation of the references to colour in this figure legend, the reader is referred to the web version of this article.)

Table C.1 Minimal sizes of podosome ring proteins calculated using methodology presented in [17]. The minimal volume of space occupied by a protein with a certain mass can be calculated using equation $R_{min}[nm] = 0.066M^{\frac{1}{2}}$, where M is the mass of the protein, measured in Daltons [17].

| Protein | Mass [kDa] | R _{min} [nm] | Notes |
|----------|------------|-----------------------|---------------------------------|
| Vinculin | 117 | 3.23 | Circular only in inactive state |
| Paxillin | 69 | 2.71 | |
| Talin | 270 | 4.27 | |

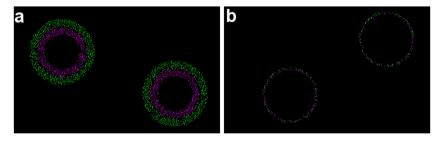


Fig. D.1. An example of simulated podosome rings. The rings were simulated as inner and outer concentric rings to correspond to the sample conditions. (a) The ration of thickness to radius is 0.6 corresponding to typical podosome ring observed with labeled samples with localization microscopy. (b) Thickness to radius ratio 0.1 corresponding to datasets analyzed with 3B method.

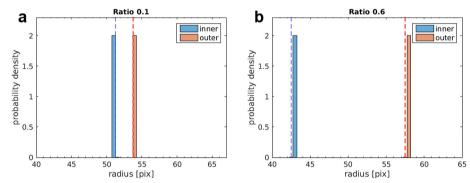


Fig. D.2. An average ring radius measured for different ratio of thickness and radius of simulated podosomes. Two values of ratio were simulated to correspond to observed average values observed in (a) 3B analyzed data sets and (b) labeled and QuickPALM analyzed localization microscopy. Podosome rings were simulated as two concentric rings corresponding to two proteins imaged for this study. Dashed lines correspond to an expected value of radius (calculated as a middle value between the ring radius). An average ring radius measured for different ratio of thickness and radius of simulated podosomes. (a) Measured average ring radius for a whole ring. (b) Inner and (c) outer concentric ring simulated to correspond to two protein imaged with localization microscopy. Dashed lines correspond to an expected value of radius (calculated as a middle value between the ring radius). Marked with blue for ration 0.6 and red for ratio 0.1. (For interpretation of the references to colour in this figure legend, the reader is referred to the web version of this article.)

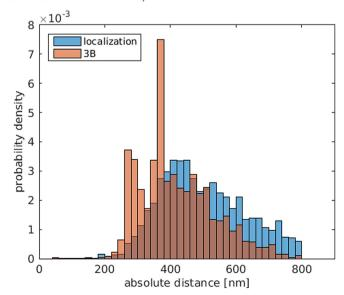


Fig. D.3. Comparison of the absolute positions of vinculin measured for localization microscopy and 3B datasets. The distributions are similar, however the distribution for localization microscopy data (blue) is shifted towards larger values. (For interpretation of the references to colour in this figure legend, the reader is referred to the web version of this article.)

measurements with similar labeling and imaging techniques which exhibit very similar thicknesses, we do not believe that this will significantly bias our relative measurement.

There is, however a significant difference observed between the thickness of the rings observed using standard localization microscopy (thicker) and 3B (thinner). When directly comparing these two measurements (see Fig. D.3 and Table D.1), it appears that the 3B measurements are biased towards smaller values as might be expected if the density on the ring is a factor. This demonstrates the need to only compare results from similar techniques for the relative measurements.

Table D.1Statistical properties of the absolute positions of vinculin imaged with localization microscopy and 3B.

| Protein | Mean distance [nm] | Median distance [nm] | Standard deviation | Quartiles |
|--------------|-----------------------|-------------------------|-----------------------|---------------|
| Localization | 512 | 489 | 142 | (420, 580) |
| 3B | 421 | 394 | 120 | (360, 500) |

References

- [1] E. Betzig, G.H. Patterson, R. Sougrat, O.W. Lindwasser, S. Olenych, J.S. Bonifacino, M.W. Davidson, J. Lippincott-Schwartz, H.F. Hess, Imaging intracellular fluorescent proteins at nanometer resolution, Science 313 (5793) (2006) 1642–1645.
- [2] M.J. Rust, M. Bates, X. Zhuang, Sub-diffraction-limit imaging by stochastic optical reconstruction microscopy (STORM), Nat. Methods 3 (10) (2006) 793– 795
- [3] A. Löschberger, S. van de Linde, M.-C. Dabauvalle, B. Rieger, M. Heilemann, G. Krohne, M. Sauer, Super-resolution imaging visualizes the eightfold symmetry of gp210 proteins around the nuclear pore complex and resolves the central channel with nanometer resolution, J. Cell Sci. 125 (9) (2011) 570–575.
- [4] A. Szymborska, A. de Marco, N. Daigle, V.C. Cordes, J.A.G. Briggs, J. Ellenberg, Nuclear pore scaffold structure analyzed by super-resolution microscopy and particle averaging, Science 341 (6146) (2013) 655–658.
- [5] M.A. Fischler, R.C. Bolles, Random sample consensus: a praradigm for model fitting with applications to image analysis and automated cartography, Commun. ACM 24 (6) (1981) 381–395.
- [6] C.L.L. Hendriks, M. van Ginkel, P.W. Verbeek, L.J. van Vliet, The generalized radon transform: sampling, accuracy and memory considerations, Pattern Recogn. 38 (12) (2005) 2494–2505.
- Recogn. 38 (12) (2005) 2494–2505.
 [7] V. Veillat, P. Spuul, T. Daubon, I. Egana, I. Kramer, E. Génot, Podosomes: multipurpose organelles?, Int J. Biochem. Cell Biol. 65 (1) (2015) 52–60.
- [8] Y. Calle, S. Burns, A.J. Thrasher, G.E. Jones, The leukocyte podosome, Eur. J. Cell Biol. 85 (3–4) (2006) 151–157.
- [9] J. Monypenny, H.-C. Chou, I. Banón-Rodríguez, A.J. Thrasher, G.E.J. Inés, M. Antónb, Y. Calle, Role of wasp in cell polarity and podosome dynamics of myeloid cells, Eur. J. Cell Biol. 90 (2–3) (2011) 198–204.
 [10] M.B. Meddens, B. Rieger, C.G. Figdora, A. Cambi, K. van den Dries, Automated
- [10] M.B. Meddens, B. Rieger, C.G. Figdora, A. Cambi, K. van den Dries, Automated podosome identification and characterization in fluorescence microscopy, Microsc. Microanal. 19 (1) (2013) 180–189.
- [11] S. Cox, E. Rosten, J. Monypenny, T. Jovanovic-Talisman, D.T. Burnette, J. Lippincott-Schwartz, G.E. Jones, R. Heintzmann, Bayesian localization

- microscopy reveals nanoscale podosome dynamics, Nat. Methods 9 (2) (2012) 195–200
- [12] M.B. Meddens, K. van den Dries, A. Cambi, Podosomes revealed by advanced bioimaging: what did we learn?, Eur J. Cell Biol. 93 (10) (2014) 380–387.
- [13] V. Vijayakumar, J. Monypenny, X.J. Chen, L. Machesky, S. Lilla, A.J. Thrasher, I. M. Antn, Y. Calle, G.E. Jones, Tyrosine phosphorylation of WIP releases bound WASP and impairs podosome assembly in macrophages, J. Cell Sci. (2014), http://dx.doi.org/10.1242/jcs.154880. http://jcs.biologists.org/content/early/2014/11/13/jcs.154880.
- [14] Nikon, Super Resolution Microscope N-STORM. STORM Protocol-Sample Preparation, [Online; retrieved on 10th of November 2015], 2015. https://nic.med.harvard.edu/files/userfiles/N-STORM%205AMPLE%20PREP.pdf.
- [15] R. Dave, D.S. Terry, J.B. Munro, S.C. Blanchard, Mitigating unwanted photophysical processes for improved single-molecule fluorescence imaging, Biophys. J. 96 (6) (2009) 2371–2381.
- [16] R. Henriques, M. Lelek, E.F. Fornasiero, F. Valtorta, C. Zimmer, M.M. Mhlanga, QuickPALM: 3D real-time photoactivation nanoscopy image processing in ImageJ, Nat. Methods 7 (5) (2010) 339–340.
- [17] H.P. Erickson, Size and shape of protein molecules at the nanometer level determined by sedimentation, gel filtration, and electron microscopy, Biol. Proced. Online 11 (1) (2009) 32–51.
- [18] K.A.K. Tanaka, K.G.N. Suzuki, Y.M. Shirai, S.T. Shibutani, M.S.H. Miyahara, H. Tsuboi, M. Yahara, A. Yoshimura, S. Mayor, T.K. Fujiwara, A. Kusumi, Membrane molecules mobile even after chemical fixation, Nat. Methods 7 (11) (2010) 865–866.
- [19] A. Shivanandan, H. Deschout, M. Scarselli, A. Radenovic, Challenges in quantitative single molecule localization microscopy, FEBS Lett. 588 (19) (2014) 3595–3602.
- [20] R.E. Thompson, D.R. Larson, W.W. Webb, Precise nanometer localization analysis for individual fluorescent probes, Biophys. J. 82 (5) (2002) 2775– 2783
- [21] R.J. Ober, S. Ram, E.S. Ward, Localization accuracy in single-molecule micorscopy, Biophys. J. 86 (2) (2004) 1185–1200.